

# Huge Scale Tests of All-Steel Multi-curve Buckling Restrained Braces

**C. S. Tsai**

*Department of Civil Engineering, Feng Chia University, Taichung, Taiwan*

**H. C. Su**

*Department of Water Resources Engineering and Conservation, Feng Chia University, Taichung, Taiwan*

**T. C. Chiang**

*Technical Manager, Earthquake Proof Systems, Inc., Taichung, Taiwan*



## SUMMARY:

In this study, we propose an all-steel BRB called the multi-curve buckling-restrained brace (MC-BRB) to overcome the shortcomings of traditional BRBs that use mortar encased in a steel tube. This new BRB consists of double core plates, each with multiple neck portions, enlarged segment, lateral support elements, and constraining elements. The enlarged segment can be connected to the lateral support and constraining elements to increase buckling strength and prevent the lateral support and constraining elements from sliding during earthquakes. The lateral support elements can be windowed to allow quality control checks to be performed and the condition of the core plate to be monitored after an earthquake. A huge-scale component test was carried out to investigate the behavior of the new BRB. A comparison of the experimental results and theoretical calculations indicate that the all-steel MC-BRB possesses a stable and predictable mechanical behavior under cyclic loadings.

*Keywords: Buckling restrained brace, multi-curve BRB, energy dissipation device, damper, structural control*

## 1. INTRODUCTION

Since the 1970s, there has been extensive research into the prevention of the traditional brace from buckling in repeated compression during an earthquake, which is the source of stiffness and strength degradation. Wakabayashi et al. (1973) conducted a component test of the buckling-restrained brace (BRB) while using different de-bonding materials between the brace and the buckling-restraint unit to reduce the friction. Kimura et al. (1976) carried out a component test of the steel brace encased in a mortar-filled steel tube subjected to cyclic loadings. Mochizuki et al. (1979) performed tests on similar braces with a layer of shock-absorbing material to avoid adhesion between the steel and the concrete and to allow transverse expansion of the steel core in compression. This type of brace has been termed the “unbonded” brace because of the layer of “unbonding” material at the steel concrete interface. Wada et al. (1992) demonstrated that the BRB could be designed as a damper to dissipate seismic energy. A BRB or an unbonded brace basically is composed of three components: the steel core member, buckling-restraining part, and de-bonding material. Black et al. (2002) and Merritt et al. (2003) carried out standard and low-cycle fatigue tests of BRBs to examine their behavior. However, several shortcomings need to be addressed regarding traditional BRBs that use mortar encased in a steel tube to prevent the core plate from buckling. These shortcomings include the complexity of interfaces between adopted materials, uncertain precision and time consumption during the manufacturing processes and difficulties in detecting the level of damage after an earthquake has occurred.

As an alternative, all-steel buckling-restraint systems, which do not need un-bonding materials, mortar, or complicated manufacturing interfaces among different materials, have been developed to conquer the abovementioned disadvantages of traditional BRBs (Chen 2000, Tsai et al. 2004, 2005, 2006, 2008, 2009, Ma et al. 2008, Eryasar and TopKara 2010). The steel core is typically separated from the steel buckling-restraint unit by a small void in the necessary direction. All-steel BRBs can also be demountable if bolted connections between the steel core and the buckling-restraint unit are used, thus enabling inspection and monitoring. Tsai et al. (2008, 2009) proposed a new type of

all-steel BRB called the multi-curve BRB (MC-BRB) that consists of a single steel core plate with an enlarged segment in the middle length to form a multi-curved shape for the steel core, and the buckling-restraint unit that includes constraining elements and lateral support elements. Twenty five buildings in Taiwan and two in China have implemented this type of BRB (Earthquake Proof Systems, Inc.). Zhao et al. (2011) have also published the follow-up research of the MC-BRB to conclude that the MC-BRB has more stable mechanical characteristics than the traditional BRBs and does not require de-bonding material (Tsai et al. 2009, Zhao et al. 2011). However, there exist few, if any, large-scale tests, in terms of axial forces, for all-steel BRBs.

To examine the behavior of the large-scale all-steel MC-BRB, component tests of an all-steel MC-BRB designed to sustain an axial force of 14000 kN have been carried out in the Material Experimental Center at the Architecture and Building Research Institute, Ministry of the Interior, Taiwan. The results from the component tests demonstrate that the all-steel MC-BRB with double steel core plates possesses a stable behavior under cyclic loadings, providing excellent inelastic deformation capacity. Furthermore, the comparisons between the experimental results and numerical results calculated from derived mathematical formulations in this study reveal that the mechanical behavior of the all-steel MC-BRB with double steel core plates can be well predicted by the proposed formulations.

## 2. ALL-STEEL MULTI-CURVE BUCKLING RESTRAINED BRACE WITH DOUBLE CORE PLATES

As shown in Figures 2.1–2.9 the all-steel MC-BRB consists of double flat steel core plates, the buckling-restraint unit, and an insert plate located between the two core plates. The cross sections of A-A and B-B of the specimen are shown in Figures 2.3 and 2.4. Each steel core plate has a multi-curved shape through an enlarged segment, as shown in Figures 2.2-2.5, in the middle length of the MC-BRB to construct two energy dissipation segments. Figures 2.6 and 2.7 respectively show the details of the lateral support and constraining elements. Table 2.1 shows the dimensions of the tested all-steel MC-BRB specimen. The steel core plates of the MC-BRB were made of A572 (Grade 50) with a nominal yield stress of 35 kN/cm<sup>2</sup>. The size of the energy dissipation segment was 285.7 mm in width and 50 mm in thickness, which resulted in a nominal yield force of 5000 kN. Two flat steel core plates leading to the yield force of 10000 kN were adopted to avoid welding at energy dissipation segments such as the cruciform cross section. No necessary welding at major portions such as energy dissipation segments of the steel core plate makes the properties of the BRB such as the yield force and yield displacement more predictable than those using cruciform cross sections that require welding at the energy dissipation segments. The theoretical elastic stiffness of the double core MC-BRB was 16253 kN/cm. The nominal yield displacement was 6.15 mm. It should be noted that two flat steel core plates have been adopted for large axial loads in this study and that one flat steel core plate would be sufficient for smaller axial loads. As indicated in Figures 2.3, 2.4 and 2.7, the buckling-restraint unit included constraining elements that can be of any cross-sectional shape, such as that of a rectangular box, a channel, or an I section, and lateral support elements to prevent the steel core plate from global and local buckling. As indicated in Figures 2.3 and 2.8, the insert plate that can be composed of one plate or two plates was located in the middle of the cross section of the MC-BRB to separate the two flat steel core plates for easing the connection between the MC-BRB and the gusset plate stemmed from the beam and column. Note that the enlarged segments can be welded to the buckling-restraint unit to have higher buckling strength, and that the connection between the lateral support elements and the insert plate can be welding, bolting, or the combination of welding and bolting to make the connection completely or partially demountable for checking and monitoring.

Watanabe et al. (1988) suggested that the buckling-restraint unit be properly designed not to resist any significant axial load and to have sufficient flexural stiffness to avoid global buckling of BRBs, which is expressed as

$$\frac{P_{cr}}{P_{ysc}} \geq 1.5 \quad (2.1)$$

where  $P_{cr}$  is the elastic buckling strength of the buckling-restraint unit, and  $P_{ysc}$  is the yield force of the steel core.

If one steel core plate is adopted, the elastic stiffness of the MC-BRB,  $K_e$ , in terms of relative displacement between two ends defining the deformation of the BRB, can be obtained as follows (Tsai et al. 2009):

$$k_e = \frac{k_1 k_2 k_3 k_7 k_8}{(2k_2 k_3 k_7 k_8 + 2k_1 k_3 k_7 k_8 + 2k_1 k_2 k_7 k_8 + 2k_1 k_2 k_3 k_7 + k_1 k_2 k_3 k_8)} \quad (2.2)$$

where

$$k_1 = \frac{EA_1}{L_1}; k_3 = \frac{EA_3}{L_3}; k_7 = \frac{EA_7}{L_7}; k_2 = \frac{E(A_1 - A_3)}{L_2(\ln A_1 - \ln A_3)}; \text{ and } k_8 = \frac{E(A_m - A_1)}{L_8(\ln A_m - \ln A_1)}$$

where  $L_1$ ,  $L_2$ ,  $L_3$ ,  $L_7$ , and  $L_8$  are the lengths of the energy dissipation segment, first transformed segment, brace projection, enlarged segment, and second transformed segment, respectively.  $A_1$ ,  $A_3$ , and  $A_7$  are the cross-sectional areas of the energy dissipation segment, brace projection, and enlarged segment, respectively.  $A_m$  is the largest cross-sectional area of the second transformed segment.  $P$  is the axial force of the member, and  $E$  is the modulus of elasticity.

If one steel core plate is used, the relationship of nodal forces to nodal displacements at both ends of the MC-BRB is given by

$$\begin{Bmatrix} F_1 \\ F_2 \end{Bmatrix} = \begin{bmatrix} K_e & -K_e \\ -K_e & K_e \end{bmatrix} \begin{Bmatrix} u_1 \\ u_2 \end{Bmatrix} = K_{BRB} \begin{Bmatrix} u_1 \\ u_2 \end{Bmatrix} \quad (2.3)$$

where the elastic stiffness of the MC-BRB,  $K_{BRB}$ , can be expressed as

$$K_{BRB} = \begin{bmatrix} K_e & -K_e \\ -K_e & K_e \end{bmatrix} \quad (2.4)$$

where  $F_1$  and  $F_2$  denote nodal forces at both ends of the MC-BRB; and  $u_1$  and  $u_2$  are nodal displacements at both ends of the MC-BRB. Note that if double steel core plates are used, the stiffness derived above should be doubled.

### 3. EXPERIMENTAL RESULTS AND DISCUSSION

According to the Recommended Provisions for Buckling-Restrained Braces (AISC 2005), the design of braces shall be based upon results from qualifying cyclic tests in accordance with the procedures and acceptance criteria contained in the Provisions' Appendix.

According to the Recommended Provisions (AISC 2005), the following loading sequence that includes the standard loading protocol and low-cycle fatigue loading protocol shall be applied to the test specimen, where the deformation is the axial deformation of the core plate:

- (1) 2 cycles of loading at the deformation corresponding to  $\Delta_{by}$ ,
- (2) 2 cycles of loading at the deformation corresponding to  $0.5 \Delta_{bm}$ ,
- (3) 2 cycles of loading at the deformation corresponding to  $1.0 \Delta_{bm}$ ,
- (4) 2 cycles of loading at the deformation corresponding to  $1.5 \Delta_{bm}$ ,

(5) 2 cycles of loading at the deformation corresponding to  $2.0 \Delta_{bm}$ , and

(6) Additional complete cycles of loading at the deformation corresponding to  $1.5 \Delta_{bm}$  as required for the Brace Test Specimen to achieve a cumulative inelastic axial deformation of at least 200 times the yield deformation.  $\Delta_{by}$  denotes the axial deformation at first significant yield of the specimen, and  $\Delta_{bm}$  depicts the axial deformation of the specimen at the design story drift.

The loading sequence of the 2005 AISC Provisions is summarized in Figure 3.1. The AISC Recommended Provision defines the compression strength adjustment factor,  $\beta$ , as

$$\beta = \frac{P_{max}}{T_{max}} \quad (3.1)$$

where  $P_{max}$  is the maximum compressive force; and  $T_{max}$  is the maximum tensile force corresponding to  $1.5 \Delta_{bm}$ . While a large deformation occurs in the longitudinal direction of a brace, the changes of the cross-sectional area and the length of the member should be taken into consideration. In theory, the compression strength adjustment factor,  $\beta$ , can be approximately obtained by the procedures as follows:

The cross-sectional area of the energy dissipation segment of the BRB under a large deformation in compression,  $A_{com}$ , can be expressed as

$$A_{com} = A_0 (I + \nu \varepsilon)^2 \quad (3.2)$$

and the length of the energy dissipation segment in compression,  $l_{com}$ , is

$$l_{com} = l_0 (I - \varepsilon) \quad (3.3)$$

where  $A_0$  and  $l_0$  are the original cross-sectional area and original length of the energy dissipation segment, respectively;  $\nu$  is Poisson's ratio, and  $\varepsilon$  is the tested strain of the energy dissipation segment.

Therefore, the elasto-plastic stiffness of the energy dissipation segment,  $K_{com}$ , of the BRB at the tested strain in compression is given by

$$K_{com} = \frac{E_{ep} A_{com}}{l_{com}} = \frac{E_{ep} A_0 (I + \nu \varepsilon)^2}{l_0 (I - \varepsilon)} \quad (3.4)$$

where  $E_{ep}$  is the elasto-plastic modulus of the energy dissipation segment at the tested strain.

Similarly, the elasto-plastic stiffness of the energy dissipation segment,  $K_{ten}$ , of the BRB at the tested strain in tension can be obtained as

$$K_{ten} = \frac{E_{ep} A_{ten}}{l_{ten}} = \frac{E_{ep} A_0 (I - \nu \varepsilon)^2}{l_0 (I + \varepsilon)} \quad (3.5)$$

where  $A_{ten}$  and  $l_{ten}$  are the cross-sectional area and length of the energy dissipation segment in tension at the tested strain, respectively.

Therefore, the ratio of the elasto-plastic stiffness in compression to that in tension at the tested strain,  $R_{stiff}$ , is expressed as

$$R_{stiff} = \frac{K_{com}}{K_{ten}} = \frac{\frac{E_{ep} A_0 (I + v\varepsilon)^2}{l_0 (I - \varepsilon)}}{\frac{E_{ep} A_0 (I - v\varepsilon)^2}{l_0 (I + \varepsilon)}} = \frac{(I + v\varepsilon)^2 (I + \varepsilon)}{(I - v\varepsilon)^2 (I - \varepsilon)} \quad (3.6)$$

If  $\nu = 0.5$  (incompressible material) is assumed at large deformations, then  $R_{stiff}$  is given by

$$R_{stiff} = \frac{(I + 0.5\varepsilon)^2 (I + \varepsilon)}{(I - 0.5\varepsilon)^2 (I - \varepsilon)} \approx I + 4\varepsilon + 8\varepsilon^2 \approx (I + 2\varepsilon)^2 \quad (3.7)$$

If the energy dissipation segment is subjected to identical deformations in both tension and compression without local and global buckling, the theoretical compression strength adjustment factor,  $\beta$ , will be equal to  $R_{stiff}$ ; that is,

$$\beta = R_{stiff} \approx I + 4\varepsilon + 8\varepsilon^2 \approx (I + 2\varepsilon)^2 \quad (3.8)$$

The AISC Provisions (2005) require that the value of cumulative inelastic axial deformation capacity,  $\eta$ , for uniaxial testing of BRBs be at least 200.

As shown in Figure 3.2, the testing facility is located in the Material Experimental Center at Architecture and Building Research Institute, Ministry of the Interior, Taiwan. The loading capacities of the test machine are 30 MN in compression and 15 MN in tension. The specimen was placed vertically, as shown in Figures 3.2 and 3.3. The load-deformation responses of the standard test of the specimen are shown in Figure 3.4. The axial deformation in Figure 3.4 represents the sum of the displacements at both ends of the MC-BRB. There existed a flat in the early two nonlinear cycles because the strains in these two cycles were still within the plateau area of the stress-strain curve of the material. The measured elastic stiffness was 16618 kN/cm, which was 2.2% higher than the theoretical value of 16253 kN/cm calculated from Eqs. (2.2) and (2.4). The measured yield force was 10353 kN, which was 3.5% larger than the theoretical value of 10000 kN. The measured yield displacement was 6.23 mm, which was 1.28% larger than the theoretical value of 6.15 mm. Table 3.1 summarizes the comparison of measured data and theoretical values calculated from the mathematical formulations derived above. The tested maximum strain in the regions of energy dissipation segments of the specimen was 2.6%. The measured maximum compressive and tensile forces at the strain of 2.6% were 13934 kN and 12573 kN, respectively. The compression strength adjustment factor,  $\beta$ , was 1.1082, which was much smaller than the value ( $<1.30$ ) required by the 2005 AISC Provisions, and the tension strength adjustment factor,  $\omega$ , which is the ratio of the maximum tensile force to the nominal yield force, was 1.2573 at strain of 2.6%. Table 3.2 lists the comparison of the measured compression strength adjustment factor,  $\beta$ , and theoretical values calculated from Eq. (3.8). It can be concluded from the comparison of data in Table 3.2 that the numerical results of the compression strength adjustment factor calculated from the proposed mathematical formulation are in very good agreement with the experimental results. Twenty-six cycles of hysteresis loops presented in Figure 3.5 give the results of the low-cycle fatigue test. The cumulative inelastic axial deformation capacity,  $\eta$ , representing the ratio of the accumulated inelastic deformation until failure of the tested specimen to the yield deformation, was 567.8, which was much higher than the value of at least 200 required by the 2005 AISC Provisions. Figure 3.6 demonstrates that the exterior of the MC-BRB had no sign of damage or yielding after complete testing. Figure 3.7 shows necking and rupture in one energy dissipation segment of the steel core close to the transformed segment occurred during tensile loading at the last cycle of fatigue testing. Figures 3.8–3.10 indicate that there was no sign of local and global buckling at the steel core plates, constraining elements or lateral support elements, and no sign of damage at the buckling-restraint unit. Based on the experimental observations, the wall of the constraining element provided good support to the steel core without yielding. No slipping between the steel core plates and the buckling-restraint unit was observed because of the welding between the enlarged segment of the steel core plate and the buckling-restraint unit. These test results showed excellent stable hysteretic behavior, satisfactory inelastic axial deformation capacity, and predictable

elastic stiffness, yield displacement, yield force, and compression strength adjustment factor that can be calculated in theory.

#### 4. CONCLUSIONS

A large-scale all-steel multi-curve buckling-restrained brace (MC-BRB) with double core plates was investigated experimentally. Based on the experimental results and observations, no sign of global or local buckling was observed, and the buckling-restraint unit provided good support to the steel core plates without any damage. The comparisons between test results and theoretical calculations reveal that the mathematical formulations derived in this study can well predict the behavior of the MC-BRB. Experimental results suggest that no welding at the major portions of the steel core plate, such as the energy dissipation segments, makes the mechanical behavior of the BRB more predictable. Welding the enlarged segment located in the middle of the steel core plate to the buckling-restraint unit was found to be a suitable option for preventing slipping of the buckling-restraint unit. Satisfactory adjustment factors were obtained based on the comparisons of experimental results with the 2005 AISC Provisions. A properly designed all-steel multi-curve buckling-restrained brace with double core plates possessed stable mechanical behavior with excellent hysteresis.

#### REFERENCES

- AISC (2005). Seismic provisions for structural steel buildings. Appendix, Part I, AISC.
- Black, C. J., Makris, N. and Aiken, I. D. (2002). Component testing, stability analysis and characterization of buckling-restrained braces. *Journal of Structural Engineering: ASCE*, **130**: 6, 880-894, USA.
- Chen, C.C. (2000). Seismic behavior and design of buckling inhibited braces and ductile CBF's. *Structural Engineering* **15**:1, 53-78, in Chinese.
- Earthquake Proof Systems, Inc. (2012), Taichung, Taiwan, <http://www.epstw.com/>.
- Eryasar, M. and Topkara, C. (2010). An experimental study on steel-encased buckling-restrained brace hysteretic dampers. *Earthquake Engineering and Structural Dynamics*, **39**, 561-581, USA.
- Kimura, K., Yoshizaki, K. and Takeda, T. (1976). Tests on braces encased by mortar in-filled steel tubes. *Summaries of Technical Papers of Annual Meeting*, Architectural Institute of Japan, 1041-1042, in Japanese.
- Ma, N., Wu, B., Zhao, J., Li, H., Ou, J. and Yang, W. (2008). Full scale test of all-steel buckling restrained braces. Paper No. 11-0208, *the 14th World Conference on Earthquake Engineering*, Beijing, China.
- Merritt, S., Uang, C. M. and Benzoni, G. (2003). Subassembly testing of corebrace buckling-restrained braces. Department of Structural Engineering, Structural Systems Project, Report No. TR-2003/01, UC San Diego.
- Mochizuki, S., Murata, Y., Andou, N. and Takahashi, S. (1979). Experimental study on buckling of unbounded braces under axial forces: Parts 1 and 2. *Summaries of technical papers of annual meeting*. Architectural Institute of Japan, 1623-1626, in Japanese.
- Tsai, C. S., Chiang, T.C., Chen, B. J., Chen, W. S. and Yu, S. H. (2004). Component test and mathematical modeling of advanced unbonded brace. *Seismic Engineering, The 2004 ASME PVP Conference*, V. C. Matzen and S. Fujita, editors, **486**:2, 231-236, California, U. S. A.
- Tsai, C. S., Chen, W. S. and Chen, K. C. (2005). Shaking table test of structure with reinforced buckling restrained braces. *Seismic Engineering, The 2005 ASME PVP Conference*, C. S. Tsai, editor, Denver, **8**, 307-312, Colorado, U.S.A.
- Tsai, C. S., Chen, W. S. and Chen, B. J. (2006). Component tests and simulation of advanced buckling restrained braces. *ASME 2006 Pressure Vessels and Piping Conference*, Vancouver, Canada, PVP2006-ICPVT11-93491.
- Tsai, C. S., Chen, W. S. and Lin, Y. C. (2008). Full scale shaking table tests of a steel structure with multi-curve buckling restrained braces. Paper No. 05-06-0007, *the 14th World Conference on Earthquake Engineering*, Beijing, China.
- Tsai, C. S., Lin, Y. C., Chen, W. S. and Su, H. C. (2009). Mathematical modeling and full-scale shaking table tests for multi-curve buckling restrained braces. *Earthquake Engineering and Engineering Vibration* **8**: 3, 359-371.
- Wada, A., Connor, J., Kawai, H., Iwata, M. and Watanabe, A. (1992). Damage tolerant structures. *Proceeding 5th U.S.-Japan Workshop on the Improvement of Structural Design and Construction Practices*, Applied Technology Council, **ATC-15-4**, 27-39, San Diego, CA.

Wakabayashi, M., Nakamura, T., Kashibara, A., Morizono, T. and Yokoyama, H. (1973). Experimental study of elasto-plastic properties of precast concrete wall panels with built-in insulating braces. *Summaries of Technical Papers of Annual Meeting*, Architectural Institute of Japan, Structural Engineering Section 10: 1041-1044, in Japanese.

Watanabe, A., Hitomi, Y., Saeki, E., Wada, A. and Fujimoto, M. (1988). Properties of brace encased in buckling-restraining concrete and steel tube. *Proceedings of the 9th World Conference on Earthquake Engineerin: IV*, Tokyo.

Zhao, J., Wu, B. and Ou, J. (2011). A novel type of angle steel buckling-restrained brace: cyclic behavior and failure mechanism. *Earthquake Engineering and Structural Dynamics*, **40**, 1083-1102.

**Table 2.1.** Dimensions of All-Steel BRB (unit: mm)

|       |     |     |     |       |       |       |       |     |
|-------|-----|-----|-----|-------|-------|-------|-------|-----|
| Lw    | L1  | L2  | L3  | L4    | L5    | L6    | L7    | B   |
| 4500  | 950 | 360 | 480 | 1700  | 850   | 3600  | 200   | 140 |
| B1    | B2  | B3  | B4  | B5    | b     | b1    | b2    | b3  |
| 285.7 | 430 | 516 | 50  | 115.2 | 169.2 | 115.2 | 131.2 | 54  |
| b4    | H   | H1  | R1  | tz    | tw1   | tc    | t     | Ls  |
| 38    | 570 | 630 | 100 | 80    | 14    | 50    | 50    | 840 |
| ts    | Hs  | g   | N   | N1    | B6    | Lg    | tw2   | L8  |
| 50    | 121 | 50  | 2   | 2     | 90    | 890   | 22    | 360 |

**Table 3.1.** Comparison of Measured and Theoretical Parameters

| Items                     | Measured Data | Theoretical Values | Errors |
|---------------------------|---------------|--------------------|--------|
| Elastic Stiffness (kN/cm) | 16618         | 16253              | 2.2%   |
| Yield Force (kN)          | 10353         | 10000              | 3.5%   |
| Yield Displacement (mm)   | 6.23          | 6.15               | 1.28%  |

**Table 3.2.** Comparison of Measured and Theoretical Compression Strength Adjustment Factors ( $\beta$ )

| Strain (%) | Measured $\beta$ | Theoretical $\beta$ | Errors |
|------------|------------------|---------------------|--------|
| 1.35       | 1.0637           | 1.0555              | 0.77%  |
| 2.00       | 1.0746           | 1.0832              | 0.80%  |
| 2.60       | 1.1082           | 1.1094              | 0.11%  |

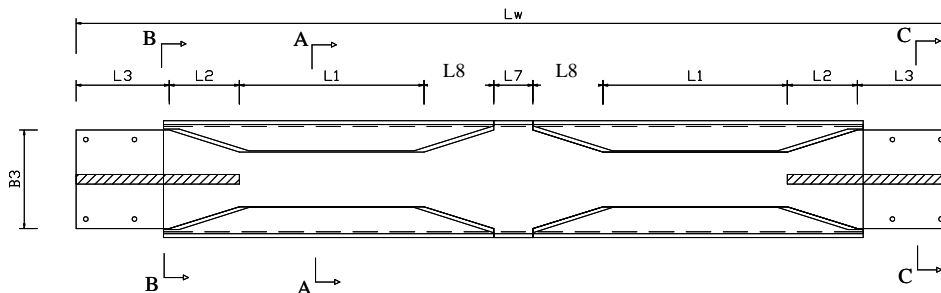


**Figure 2.1.** All-Steel Multi-Curve Buckling Restrained Brace with Double Cores (Cross sections are shown in Figures 2.3 and 2.4)

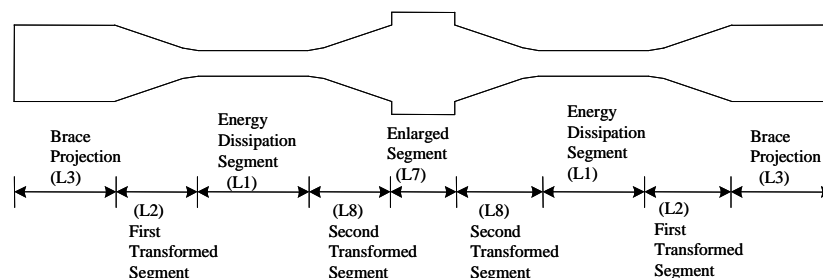


**Figure 2.2.** Details of Each of Double Flat Steel Core Plates of the MC-BRB

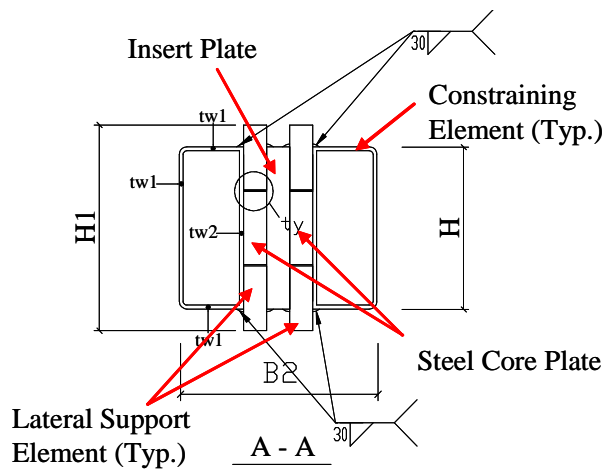


**Figure 2.3.** Details of Section A-A

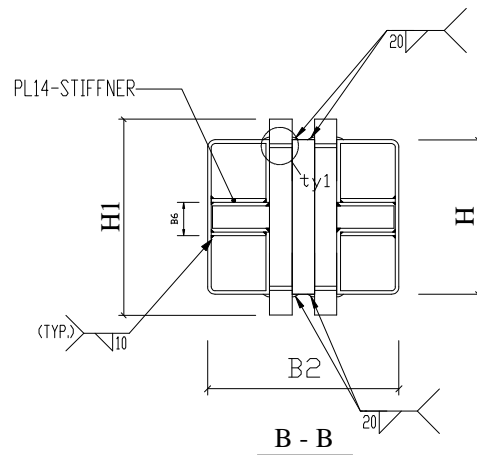


**Figure 2.4.** Details of Section B-B

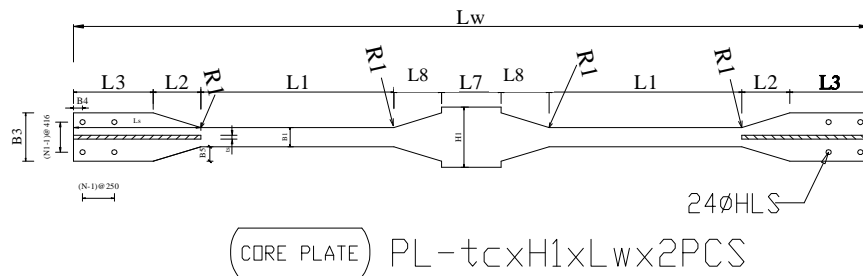


**Figure 2.5.** Dimensions of the Flat Steel Core Plate with Stiffener at Both Ends

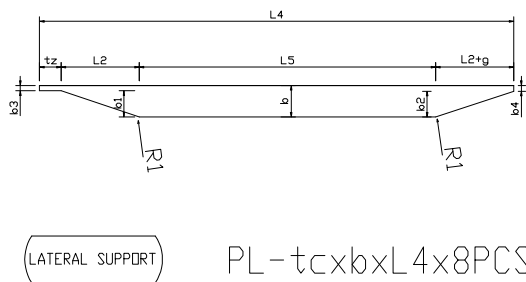


**Figure 2.6.** Details of the Lateral Support Element (referring to Figures 2.1 and 2.3)

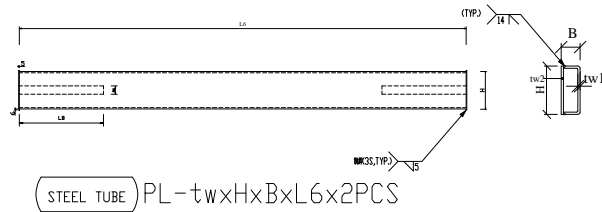


**Figure 2.7.** Details of the Constraining Element (referring to Figures 2.1 and 2.3)



**Figure 2.8.** Details of the Insert Plate

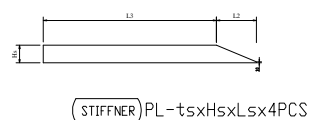


**Figure 2.9.** Details of the Stiffener of Section C-C

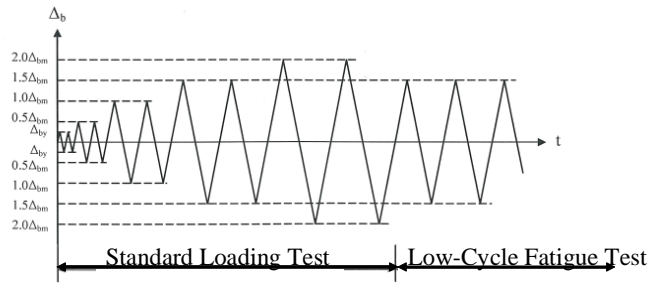


**Figure 3.1.** Loading Sequence According to AISC Provisions (2005)



**Figure 3.2.** Test Set-Up of the All-Steel MC-BRB



**Figure 3.3.** Picture for the Bottom End of the All-Steel MC-BRB Before Testing

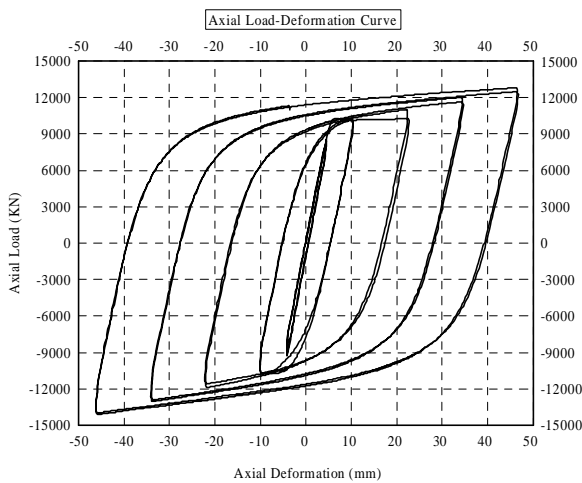


**Figure 3.4.** Hysteretic Loops of the Standard Test of the All-Steel MC-BRB

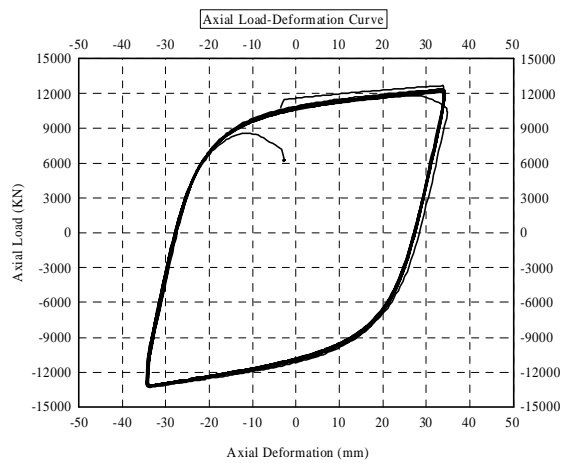


**Figure 3.5.** Hysteretic Loops of the Low Cycle Fatigue Test of All-Steel MC-BRB



**Figure 3.6.** Picture for the Bottom End of the All-Steel MC-BRB After Testing



**Figure 3.7.** Necking and Rupture at the Bottom End of the Right Energy Dissipation Segment of the Steel Core During Tensile Loading



**Figure 3.8.** Open-up View of the Bottom End of the Left Energy Dissipation Segment of the All-Steel BRB After Testing



**Figure 3.9.** Open-up View of the Top End of the Left Energy Dissipation Segment After Testing



**Figure 3.10.** Open-up View of the Top End of the Right Energy Dissipation Segment After Testing